論 文 の 内 容 の 要 旨

論文題目 **Two-dimensional transition metal carbides MXenes as a charge storage host in hydrate melt electrolyte**
（常温溶融水和物中での二次元遷移金属炭化物MXeneの電荷貯蔵機能）

氏　　名　　金 基宰

1. Introduction

Supercapacitors are capble of quick charge storage through fast electric double-layer (EDL) formation without ion-diffusion limitation or structural changes, which achieves higher power density and better cycle retention compared to Li-ion batteries. In particular, for a grid-scale use, aqueous supercapacitors comprising of inexpensive aqueous electrolytes are attractive in terms of cost. However, the electrochemical potental window of water is so narrow that the operation votlage and hence the energy density of the aqueous capacitors are low.

To undermine this obstacle, highly-concentrated aqueous electrolytes ($Li(TFSI)_{0.7}(BETI)_{0.3}{\cdot}2H_2O$, hydrate-melt)[1] are focused in this work. The hydrate-melt electrolyte has a wide electrochemical potential window exceeding the thermodynamic hydrogen/oxygen evolution limits of a free water molecule, because all the water molecules are coordinated to Li^+. Therefore, aqueous supercapacitors using the hydrate-melt electrolytes are expected to provide high operation voltage leading to high energy density.

As for an electrode material for the hydrate-melt aqueous electrolytes, 2D transition-metal carbides called MXenes are used.[2] Intercalation EDL capacitance of MXenes, which provides large amounts of charge storage and fast charge/discharge capability, can maximize the electrochemical performances with hydrate melt. MXenes $M_{n+1}X_nT_x$ (M: Ti, Nb, Mo, V, *etc.*; X: C, N; *n*: 1, 2, or 3; T_x, surface termination group: OH, O, F, Cl) are two-dimensional (2D) layered materials prepared by removing A layers from MAX phases $M_{n+1}AX_n$ (A: 3A or 4A Group such as Al, Ga, Si, Ge, *etc.*). MXenes are reported to provide a large capacitance greater than 300 F/g in aqueous system, and thus suitable to achieving aqueous supercapacitors with high energy density.[3]

This work aims to develop high-voltage aqueous supercapacitors consisting of MXene electrodes and a hydrate-melt electrolyte. Furthermore, interfacial charge transfer in MXene with aqueous electrolytes was investigated to understand the effect of electrolyte concentrations. Lastly, synthesis of MBenes (2D transion-metal borides), which have been predicted as promising candidates for supercapacitors due to large charge storage ability and low diffusion energy barrier,[4] were challenged with intensive etching process of a MAB phases.

2. Dense charge accumulation in MXenes with hydrate melt electrolyte

The MAX phase Ti_2AlC was prepared using a high-frequency induction furnace at 1350 ˚C for 1 h. Since Ti-C bonds are stronger than Ti-Al bonds in the MAX phase Ti_2AlC, MXene Ti_2CT_x was synthesized by selectively removing Al layers from Ti_2AlC in LiF/HCl aqueous solution.

The XRD patterns of Ti_2AlC and Ti_2CT_x are shown in **Fig. 1**. The diffraction pattern of Ti_2AlC exhibits a layered hexagonal structure with $P6_3/mmc$ symmetry. After etching process of Ti_2AlC, 002 diffraction peak of Ti_2CT_x is shifted to a lower angle side relative to

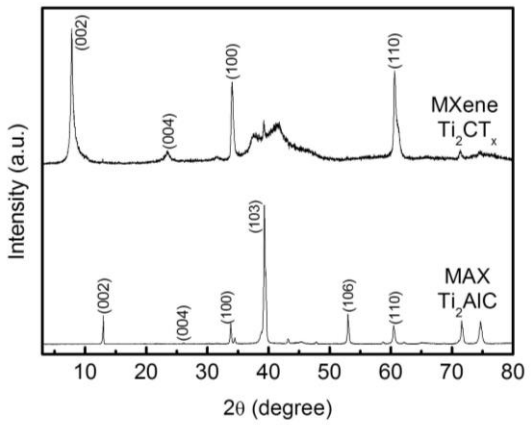

Fig. 1. XRD patterns of MAX (Ti_2AlC) and MXene (Ti_2CT_x)

that of Ti_2AlC, which corresponds to the expansion of an interlayer distance (d_{inter}) from 6.8 to 11.3Å . This d_{inter} expansion is explained by the existence of bulky surface terminal group (-OH, -O, -F, and -Cl).

Fig. 2 shows the CV curves of Ti_2CT_x with hydrate-melt and 1.0 M Li_2SO_4 electrolytes. Regardless of the electrolytes, Ti_2CT_x exhibits typical capacitive behavior with the rectangular shape of a CV curve. Notably, Ti_2CT_x with a hydrate-melt electrolyte exhibits the wide electrochemical window of 1.1 V, which is much wider than that with a 1.0 M Li_2SO_4 aqueous electrolyte. An averaged gravimetric capacitance for each electrolyte is comparable (168 and 158 F/g for a hydrate-melt electrolyte and a 1.0 M Li_2SO_4 electrolyte, respectively).

To evaluate the charge-storage capability, galvanostatic charge/discharge experiments were conducted at a specific current of 30 mA/g. Ti_2CT_x exhibits a sloping potential profile for both aqueous electrolytes, which is typical of a capacitor electrode. A specific capacity with a hydrate melt electrolyte is approximately 60 mAh/g, which is much larger than that for a 1.0 M Li_2SO_4 electrolyte (20 mAh/g), owing to the wide electrochemical window of a hydrate-melt electrolyte.

The charge-storage mechanism of Ti_2CT_x in a hydrate-melt electrolyte was examined using *ex-situ* XRD at different charge of states. The 002 diffraction peak reversibly shifts upon charging/discharging, which corresponds to the expansion/shrinkage of d_{inter} between approximately 13.7 and 14.1 Å . The reversible change of d_{inter} suggests that Ti_2CT_x exhibits intercalation/deintercalation of hydrated Li^+.

The potential profiles of Ti_2CT_x and activated carbon in a hydrate-melt electrolyte are presented in **Fig. 3a**. Both electrodes exhibit the wide operating potential windows of -1.1 V and 0.9 V for Ti_2CT_x and activated carbon, respectively. Using these electrodes, a full-cell (Ti_2CT_x|hydrate melt|AC) was fabricated with a capacity-balanced configuration as a aqueous supercapacitor. As shown in **Fig. 3b**, the full-cell provides a specific capacity of approximately 45 mAh/g per the weight of Ti_2CT_x at a specific current of 100 mA/g. The wide electrochemical potential windows of both electrodes in a hydrate-melt electrolyte enables a high averaged operation voltage of approximately 2.0 V. Furthermore, capacity retention is approximately 100% even after 1000 cycles with the coulombic efficiency exceeding 99 % throughout the cycling. These results suggest stable operation of the Ti_2CT_x/hydrate-melt system with minimum occurrence of side reactions, such as hydrogen evolution.

Fig. 3c shows the Ragone plot of full-cell comprising a hydrate-melt electrolyte (empty) and a 1.0 M Li_2SO_4 aqueous electrolyte (filled). The full-cell with a hydrate-melt electrolyte exhibits much higher energy density of *ca.* 15 Wh/kg at the power density of 100 W/kg than that with a 1.0 M Li_2SO_4 aqueous electrolyte, owing to an expanded electrochemical window.

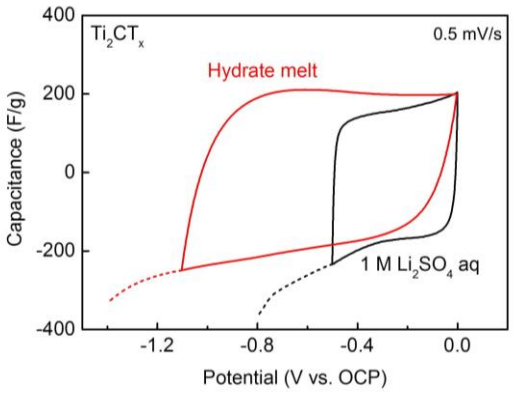

Fig. 2. CV of Ti_2CT_x using hydrate melt and 1.0 M Li_2SO_4 aqueous electrolytes

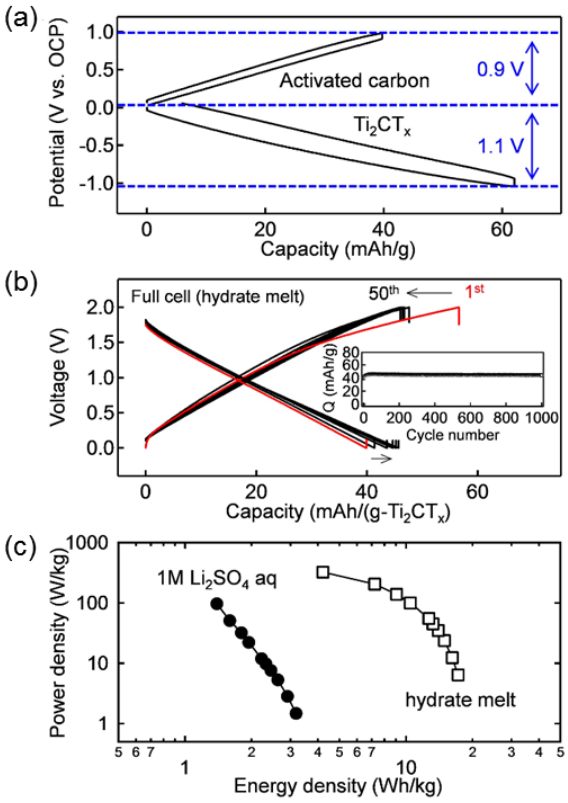

Fig. 3. (a) potential profiles of Ti_2CT_x and activated carbon using hydrate-melt. (b) Voltage profiles of a capacity-balanced full-cell consisting of a Ti_2CT_x negative electrode and an activated carbon positive electrode with a hydrate-melt electrolyte. Inset shows the cycle stability during 1000 cycles. (c) Ragone plots of Ti_2CT_x using hydrate-melt and 1.0 M Li_2SO_4

3. Interfacial charge transfer of aqueous MXene supercapacitors

For synthesis of Ti_3AlC_2, a mixture of Ti_2AlC and TiC was heated in a high frequency induction furnace at 1350 ˚C for 1 h under Ar flow. $Ti_3C_2T_x$ was synthesized by the removal of Al layers in a LiF/HCl solution. First of all, stable potential window was determined by chronoamperometry (a steady-state leak current > –10 μA/cm^2) with 1.0, 3.0, 5.2 M LiTFSI, and a hydrate melt aqueous electrolytes. Highly-concentrated electrolytes show wider operating potentials (-1.1 V vs. Ag/AgCl for a hydrate melt and -1.0 V for a 5.2 M LiTFSI) than those of dilute electrolytes (-0.8 V vs. Ag/AgCl for 1.0 and 3.0 M LiTFSI). After determination of stable potential window, cyclic voltammetry (CV) of $Ti_3C_2T_x$ electrode was measured with 1.0, 3.0, 5.2 M LiTFSI, and a hydrate melt aqueous electrolytes at various scan rates. Averaged capacitances of $Ti_3C_2T_x$ at a scan rate of 0.5 mV/s are 128.4, 126.3, 133.0, and 140.7 F/g for 1.0, 3.0, 5.0 M LiTFSI, and a hydrate melt aqueous electrolytes, respectively. Slightly higher capacitances with highly-concentrated electrolytes were observed with wide operating potential. However, increased concentration of aqueous electrolytes brings about the low averaged capacitances at high scan rates of > 10 mV/s as shown in **Fig. 4**.

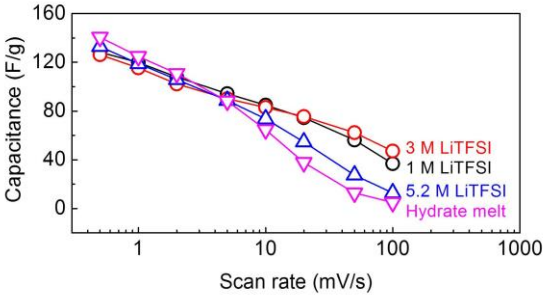

Fig. 4. Rate capability of $Ti_3C_2T_x$ with 1.0, 3.0, 5.2 M LiTFSI, and a hydrate melt aqueous electrolytes at various scan rates

Here, studies on electrochemical impedance spectroscopy (EIS) was carried out to interpret the extents of charge transfer barrier in the electrode/electrolyte interface and bulk electrolyte with dilute (1.0 and 3.0 M LiTFSI) and highly-concentrated (5.2 M LiTFSI and a hydrate melt) aqueous electrolytes under various temperatures (298, 303, 308, 313, 318 K). Interfacial charge transfer resistances of $Ti_3C_2T_x$ increase, as concentration of aqueous electrolytes increases based on EIS analysis. While charge carriers are not influenced by other chemical species in dilute system, interaction between charge carriers and other chemical species can lead to higher interfacial charge transfer resistance in highly-concentrated system.

To interpret the effects of aqueous electrolyte concentration on the activation energy (E_a) of charge transfer, R_{CT} values obtained by fitted impedance parameters using a Zview software are plotted based on Arrhenius equation ($\ln R_{CT}^{-1} = \ln A + (-E_a/1000R) \times (1000/T)$ (A: frequency factor; E_a: activation energy; R: gas constant; T: absolute temperature). The Arrhenius plot ($1000/T$ with x-axis vs. $\ln R_{CT}^{-1}$ with y-axis) can be depicted in a linear form, which could provide estimations of E_a from the slop value. E_a of bulk electrolyte were also calculated based on obtained R_S in the same manner of R_{CT}.

All E_a values of interfacial and bulk electrolyte charge transfer were calculated in **Fig. 5** as a function of H_2O/Li molar ratio. Highly-concentrated electrolytes have larger E_a values of both interfacial electrode/electrolyte ($E_{a,CT}$) and bulk electrolyte ($E_{a,S}$) charge transfer ($E_{a,CT}$: 17.4, 21.5 kJ/mol and $E_{a,S}$: 21.2, 23.0 kJ/mol for 5.2 M LiTFSI and a hydrate melt aqueous electrolytes, respectively) than those of dilute electrolytes ($E_{a,CT}$: 2.3, 4.1 kJ/mol and $E_{a,S}$: 10.5, 14.3 kJ/mol for 1.0 and 3.0 M LiTFSI aqueous electrolytes). This high energy barrier of charge transfer in highly-concentrated electrolytes gives rise to lower power density (**Fig. 4**), although they have high voltage operation and high energy density.

To understand the liquid structures and surroundings of species (water molecules, cations, anions) around the MXene $Ti_3C_2T_x$/electrolyte interface, Raman spectroscopy was measured with 1.0, 3.0, 5.2 M LiTFSI, and a hydrate melt aqueous electrolytes. With increasing concentration of LiTFSI electrolytes, the Raman peaks (746.5, 746.8, 747.9 cm^{-1} for 1.0, 3.0, 5.2 M LiTFSI aqueous electrolytes) shift to near the peak of 748.1 cm^{-1} for LiTFSI salt. It is presumed that highly-concentrated aqueous electrolytes (5.2 M LiTFSI and a hydrate melt aqueous electrolytes) cause interaction between hydrated-Li^+ and anions, which is similar characteristic with ionic bonding of LiTFSI and LiBETI salts. This interaction might disturb transportation of hydrated-Li^+ into MXene interlayers, bringing out lower power density in highly-concentrated aqueous electrolytes.

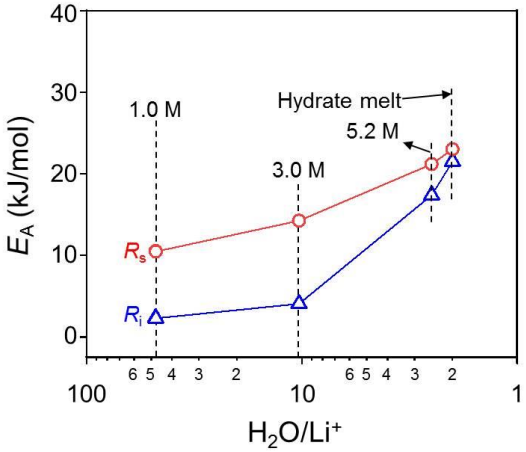

Fig. 5. Plots of activation energies (E_a) of interfacial charge transfer between $Ti_3C_2T_x$ and various aqueous electrolytes and charge transfer in bulk electrolytes as a function of H_2O/Li molar ratio.

4. Topochemical synthesis of $MoAl_{0.5}B$: A possible precursor for MBenes

A MAB phase, MoAlB with a zigzag double Al layer, was synthesized by heating the mixture of MoB and Al at 1200 ℃ for 1 h under Ar atmosphere using a high-frequency induction furnace. $MoAl_{0.5}B$ with a single Al layer was synthesized topochemically by removing Al layers from MoAlB: powdered MoAlB was treated with an etchant LiF/HCl aqueous solution. The intensive optimization of synthetic conditions determined that etching with a concentrated etchant (3 M LiF/10 M HCl solution) at elevated temperature of 40 ℃ for more than 48 h is necessary for the complete transformation. The powder X-ray diffraction (XRD) patterns in **Fig. 6** show that a 020 diffraction peak at 2θ = 12.6° for MoAlB shifts to 13.6° after the etching process. Based on the 020 diffraction corresponding to the interlayer distance (d_{inter}) of MoB layers, d_{inter} decreases from 7.1 Å to 6.4 Å, suggesting successful removal of Al layers from MoAlB.

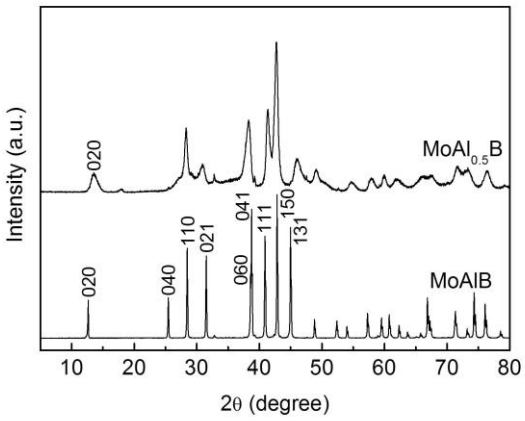

Fig. 6. XRD patterns of MoAlB and $MoAl_{0.5}B$. 020 diffraction peak shifts to higher angle, indicating shrinkage of interlayer distance due to an Al layer loss.

Indeed, energy-dispersive X-ray (EDX) analysis revealed that the atomic ratio of Mo/Al increases from 1.0 for MoAlB to 2.0 for the product, which confirms the formation of $MoAl_{0.5}B$ by the removal of Al layers from MoAlB. Importantly, as a single 020 diffraction peak was observed for the XRD pattern of the product, MoAlB was completely transformed to $MoAl_{0.5}B$. Using a MoAlB single crystal as precursor, Alameda *et al.* found the formation of several unidentified intergrowth phases of $MoAl_{0.5}B$, $MoAl_{0.66}B$, $MoAl_{0.75}B$, and $MoAl_{0.83}B$.[5] In contrast, this work successfully isolated $MoAl_{0.5}B$ under the optimized synthetic conditions including etchant concentration, temperature, and reaction duration time.

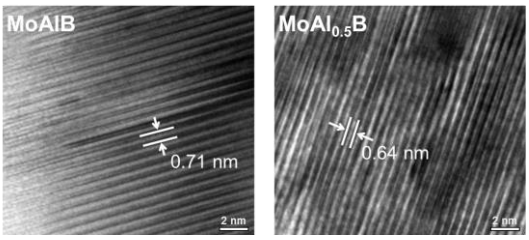

Fig. 7. TEM images of MoAlB and $MoAl_{0.5}B$

Transmission electron microscopy (TEM) images (**Fig. 7)** indicate that the layered structure of MoAlB is maintained after the etching process. The observed d_{inter} are 7.1 and 6.4 Å for MoAlB and $MoAl_{0.5}B$, respectively, which are in complete agreement with the XRD results. Therefore, all the experimental observations support that the MoAlB with a zigzag double Al layer is transformed to $MoAl_{0.5}B$ with a single Al layer topochemically, *i.e.*, maintaining the stacking structure of MoB layers. As the single Al layer of $MoAl_{0.5}B$ is identical with that of MAX phases, $MoAl_{0.5}B$ is a possible precursor for MBenes.

Reference

[1] Y. Yamada, *et al.*, *Nat. Energy* **2016**, *1*, 16129.
[2] M. R. Lukatskaya, *et al.*, *Science* **2013**, *341*, 1502.
[3] M. R. Lukatskaya, *et al.*, *Nat. Energy* **2017**, *2*, 17105.
[4] Z. Guo, *et al.*, *J. Mater. Chem. A* **2017**, *5*, 23530.
[5] L. T. Alameda, *et al.*, *J. Am. Chem. Soc.*, **2018**, *140*, 8833.